



**Three-Dimensional  $n$ th Derivative of Gaussian Separable  
Steerable Filters**

**Konstantinos G. Derpanis**

**Jacob M. Gryn**

Technical Report CS-2004-05

November 22, 2004

Department of Computer Science and Engineering  
4700 Keele Street North York, Ontario M3J 1P3 Canada

# Three-Dimensional $n$ th Derivative of Gaussian Separable Steerable Filters

Konstantinos G. Derpanis\* and Jacob M. Gryn

---

\*K.G. Derpanis gratefully acknowledges the financial support of the National Sciences and Engineering Research Council (NSERC) through their PGS B fellowship.

### **Abstract**

The following report details the construction of three-dimensional (e.g., X-Y-Z) separable steerable filters. The approach presented is an extension of the construction of two-dimensional (X-Y) separable steerable filters outlined in [6]. Additionally, three-dimensional separable steerable filters, both continuous and discrete versions, for the second derivative of the Gaussian and its Hilbert transform are reported. Experimental evaluation demonstrate that the error in the constructed separable filters are negligible. Finally, an application of the filters for surveillance based on visual motion is presented.

# 1 Introduction

In many vision and image processing tasks the application of filters at arbitrary orientations is made. For example in [1], the authors show that motion manifests itself as orientation in the spatiotemporal domain and use spatiotemporally oriented filters to detect it. A computationally expensive approach is the application of many rotated versions of a filter differing by a small rotation angle. In [6], the authors demonstrate that for a certain class of functions (i.e., filters), rotated copies can be synthesized by taking linear combinations of a small set of basis functions (i.e., the basis functions span the space of all rotations). For example, to synthesize the  $n$ th order directional derivative (in two-dimensions) of a circular-symmetric function (e.g., Gaussian) requires  $n + 1$  basis functions. Furthermore, the authors leverage the distributive property of linear filters by first convolving the input image by the set of basis functions and then realizing the required filtered version of the image by taking appropriate linear combinations of the outputs; this architecture is summarized pictorially in Fig. 1. Additionally, the authors present the construction of two-dimensional separable filters (for polynomial functions) that provide a significant gain in computational efficiency over their non-separable equivalents. The computational efficiency gain is achieved by simplifying the complexity of the two-dimensional convolution from  $O(k^2n^2)$  to  $O(kn^2)$ ; where  $k$  is the size of the filter and  $n$  is the size of the image ( $n$  by  $n$ ). Related work to the steerable filters considered in this report include, early work in image restoration (e.g., [12]) and analyzing oriented patterns (e.g., [11]), alternative analytic descriptions of steerable filters (e.g., [10, 14, 18, 22]), generating steerable filters through SVD approximations (e.g., [8, 15, 17]) and work considering various orders of Gaussian derivatives (e.g., [3, 9, 13]).

In the following report explicit forms of three-dimensional (e.g., X-Y-Z)  $n$ th degree separable steerable filters are given. The approach presented is an extension of the construction of two-dimensional (X-Y) separable steerable filters for polynomial functions outlined in [6]. As examples, both analytic and discrete forms for the second derivative of a Gaussian ( $G_2$ ) and its Hilbert transform<sup>1</sup> ( $H_2$ ) are provided. Additionally, numerical evaluations of the discrete separable versions of the  $G_2$  and  $H_2$  filters are provided. It appears that explicit analytic and numerical formulations for these filters has not previously appeared.

The organization of this report is as follows. Section 2 reviews the relevant assumptions and theorem for the construction of three-dimensional steerable filters presented in [6]. Section 3 presents the construction of X-Y-Z separable steerable filters for polynomial functions. Section 4 summarizes the separable basis functions (both continuous and discrete) for the  $G_2$  and  $H_2$  filters. Section 5 summarizes an experimental evaluation of the accuracy of the separable version of the second derivative of a Gaussian. Section 6 summarizes a surveillance application that utilizes the  $G_2$  and  $H_2$  filters. Finally, Section 7 provides concluding remarks.

---

<sup>1</sup>The Hilbert transform introduces a  $90^\circ$  phase shift to every frequency of a signal [2].

## 2 Preliminaries

In this report it is assumed that the functions to be steered are of the form of a polynomial times a separable windowing function. Additionally, the functions are assumed to have an axis of rotational symmetry<sup>2</sup>. These function, rotated by a transformation  $\mathbf{R}$  such that their axis of symmetry point along the direction cosines  $\alpha$ ,  $\beta$  and  $\gamma$ , can be written as,

$$f^{\mathbf{R}}(x, y, z) = W(r)P_N(x') \quad (1)$$

where  $W(r)$  is any spherically symmetric function (e.g., three-dimensional Gaussian-like function:  $e^{-r^2}$ ,  $r = \sqrt{x^2 + y^2 + z^2}$ ) and  $P_N(x')$  is an  $n$ th order polynomial in

$$x' = \alpha x + \beta y + \gamma z \quad (2)$$

The following theorem (Theorem 4 in [6]) provides the means for constructing steerable filters of axially symmetric three-dimensional functions (see Appendix E in [6] for proof):

**Theorem 1** *Given a three dimensional axially symmetric function  $f(x, y, z) = W(r)P_N(x)$ , where  $P_N(x)$  is an even or odd symmetry  $n$ th order polynomial in  $x$ . Let  $\alpha$ ,  $\beta$  and  $\gamma$  be the direction cosines of the axis of symmetry of  $f^{\mathbf{R}}(x, y, z)$  and  $\alpha_j$ ,  $\beta_j$  and  $\gamma_j$  be the direction cosines of the axis of symmetry of  $f^{\mathbf{R}_j}(x, y, z)$ . Then the steering equation,*

$$f^{\mathbf{R}}(x, y, z) = \sum_{j=1}^M k_j(\alpha, \beta, \gamma) f^{\mathbf{R}_j}(x, y, z), \quad (3)$$

holds if and only if

1.  $M \geq (N + 1)(N + 2)/2$  and
2. the  $k_j(\alpha, \beta, \gamma)$  satisfy

$$\begin{pmatrix} \alpha^N \\ \alpha^{N-1}\beta \\ \alpha^{N-1}\gamma \\ \alpha^{N-2}\beta^2 \\ \vdots \\ \gamma^N \end{pmatrix} = \begin{pmatrix} \alpha_1^N & \alpha_2^N & \dots & \alpha_M^N \\ \alpha_1^{N-1}\beta_1 & \alpha_2^{N-1}\beta_2 & \dots & \alpha_M^{N-1}\beta_M \\ \alpha_1^{N-1}\gamma_1 & \alpha_2^{N-1}\gamma_2 & \dots & \alpha_M^{N-1}\gamma_M \\ \alpha_1^{N-2}\beta_1^2 & \alpha_2^{N-2}\beta_2^2 & \dots & \alpha_M^{N-2}\beta_M^2 \\ \vdots & \vdots & \vdots & \vdots \\ \gamma_1^N & \gamma_2^N & \dots & \gamma_M^N \end{pmatrix} \begin{pmatrix} k_1(\alpha, \beta, \gamma) \\ k_2(\alpha, \beta, \gamma) \\ k_3(\alpha, \beta, \gamma) \\ \dots \\ k_M(\alpha, \beta, \gamma) \end{pmatrix} \quad (4)$$

## 3 Basis functions separable in X, Y and Z

In this section we provide the steering coefficients and X-Y-Z separable basis functions for some polynomial functions. The following section has been adapted from Appendix D of [6] and extended to the case of three-dimensional functions.

<sup>2</sup>Definition: An *axis of rotational symmetry* is an axis where a rotation about it results in no change of the function.

We consider the case of even or odd filters  $f^\Omega(x, y, z)$  which can be written as,

$$f^\Omega(x, y, z) = G(r)Q_N(x') \quad (5)$$

where  $G(r)$  is a separable windowing function (e.g., Gaussian-like function  $e^{-r^2} = e^{-(x^2+y^2+z^2)} = e^{-x^2}e^{-y^2}e^{-z^2}$ ) and  $Q_N(x')$  is an  $n$ th order polynomial in,

$$x' = \alpha x + \beta y + \gamma z \quad (6)$$

By Theorem 1,  $(N+1)(N+2)/2$  functions can form a basis set for  $f^\Omega(x, y, z)$ . We assume that a basis of  $M = (N+1)(N+2)/2$  X-Y-Z separable functions exists. Then there will be some set of separable basis functions  $Q_{i,j}(x)R_{i,j}(y)S_{i,j}(z)$  for which

$$f^\Omega(x, y, z) = G(r) \sum k_{i,j}(\Omega) Q_{i,j}(x) R_{i,j}(y) S_{i,j}(z) \quad (7)$$

The interpolation functions,  $k_{i,j}(\Omega)$  are found by equating the highest order products of  $x$ ,  $y$  and  $z$  in Eq. (5) with those in Eq. (7), i.e., equating the coefficients of  $x^{N-i-j}y^i z^j$  for  $\{i, j | i, j \in \mathbb{N} \text{ and } i+j \leq N\}$ . Substituting Eq. (6) into Eq. (5), yields  $M$  different products of  $x$ ,  $y$  and  $z$  of order  $N$ , since (by the specialization of the multinomial theorem [16])

$$(x')^N = \sum \frac{n!}{(n-i-j)!i!j!} \alpha^{N-i-j} \beta^i \gamma^j x^{N-i-j} y^i z^j \quad (8)$$

where the summation is taken over terms with all possible integer values of  $i$ ,  $j$  between 0 and  $N$  subject to the constraint that  $i+j \leq N$ .

Each basis function  $Q_{i,j}(x)R_{i,j}(y)S_{i,j}(z)$  can contribute only one product of powers of  $x$ ,  $y$  and  $z$  of order  $N$  (otherwise  $Q_{i,j}(x)R_{i,j}(y)S_{i,j}(z)$  would be a polynomial of  $x$ ,  $y$  and  $z$  of order higher than  $N$ ). So we have

$$Q_{i,j}(x)R_{i,j}(y)S_{i,j}(z) = c(x^{N-i-j} + \dots)(y^i + \dots)(z^j + \dots), \quad (9)$$

where  $c$  is a constant. Therefore, Eq. (5) shows that the coefficients of the highest order terms  $x^{N-i-j}y^i z^j$ , in  $f^\Omega(x, y, z)$  is

$$k_{i,j}(\alpha, \beta, \gamma) = \frac{n!}{(n-i-j)!i!j!} \alpha^{N-i-j} \beta^i \gamma^j. \quad (10)$$

Note that the lower order terms can appear in more than one separable basis function, so their coefficients will be the result of a sum of different  $k_{i,j}(\alpha, \beta, \gamma)$ .

To find the separable basis functions  $Q_{i,j}(x)R_{i,j}(y)S_{i,j}(z)$  from the original function  $f(x, y, z)$ , we note that from the steering equation for the separable basis functions, Eq. (7), we have,

$$\begin{pmatrix} f^{\Omega_1}(x, y, z) \\ f^{\Omega_2}(x, y, z) \\ \vdots \\ f^{\Omega_M}(x, y, z) \end{pmatrix} = G(r) \begin{pmatrix} \cdots & k_{i,j}(\Omega_1) & \cdots \\ \cdots & k_{i,j}(\Omega_2) & \cdots \\ \vdots & \vdots & \vdots \\ \cdots & k_{i,j}(\Omega_M) & \cdots \end{pmatrix} \begin{pmatrix} \vdots \\ Q_{i,j}(x)R_{i,j}(y)S_{i,j}(z) \\ \vdots \end{pmatrix} \quad (11)$$

The  $Q_{i,j}(x)R_{i,j}(y)S_{i,j}(z)$  can be written as a linear combination of  $f^{\Omega_j}$  by inverting the matrix of  $k_{i,j}$ 's of Eq. (11).

## 4 $G_2/H_2$ steerable quadrature filter pairs

In this section steerable filters (i.e., quadrature pairs) for both the three-dimensional  $G_2$  filter (i.e., second derivative of Gaussian) and the three-dimensional  $H_2$  filter (the Hilbert transform of the  $G_2$  filter) will be summarized.

A three-dimensional Gaussian-like function can be written as,

$$G(x, y, z) = e^{-(x^2+y^2+z^2)}. \quad (12)$$

The second derivative with respect to  $x$  of the three-dimensional Gaussian-like function is written as,

$$\frac{\partial^2 G}{\partial x^2} = (4x^2 - 2)e^{-(x^2+y^2+z^2)}. \quad (13)$$

Using Theorem 1 where  $N = 2$ , we need 6 basis functions. Tables 1, 2 and 3 were arrived at by using the construction outlined in Section 3. The direction cosines  $\alpha$ ,  $\beta$  and  $\gamma$  used were a distinct subset<sup>3</sup> of the unit normals to the faces of the dodecahedron (or the vertices of the icosahedron), which can be generated according to a cyclic permutation of  $(\pm 1, 0, \pm r)$  where  $r$  is the golden mean,  $(\sqrt{5} + 1)/2$  [19]. The dodecahedron provides a uniform 12-face tessellation of a sphere.

The Hilbert transform<sup>4</sup> of the second derivative of the three-dimensional Gaussian function is written as,

$$H_2(x, y, z) = (-2.254x + x^3)e^{-(x^2+y^2+z^2)}. \quad (14)$$

Using Theorem 1 where  $N = 3$ , we need 10 basis functions. Tables 4, 5 and 6 were arrived at by using the construction outlined in Section 3. The direction cosines  $\alpha$ ,  $\beta$  and  $\gamma$  used were a distinct subset of the normals (normalized) to the faces of the icosahedron (or the vertices of the dodecahedron), which can be generated according to a cyclic permutation of  $(0, \pm r, \pm 1/r)$  and  $(\pm 1, \pm 1, \pm 1)$  where  $r$  is the golden mean  $(\sqrt{5} + 1)/2$  [19].

## 5 Experimental evaluation

In this section the root mean square (rms) errors of the discrete separable  $G_2$  and  $H_2$  filters presented in Section 4 are reported.

For each of the filters we compared the convolution output of a test image with the rotated versions of the non-separable and separable filters. The test image used was a three-dimensional zone plate, specifically a 2D analog of the 1D linear chirp (i.e.,  $f(x) = \cos[(\omega x)x] = \cos(\omega x^2)$ , where  $\omega x$  denotes the instantaneous frequency)<sup>5</sup>, defined as,

$$\begin{aligned} f(x, y, z) &= \cos[(\omega \sqrt{x^2 + y^2 + z^2}) \sqrt{x^2 + y^2 + z^2}] \\ &= \cos[\omega(x^2 + y^2 + z^2)] \end{aligned} \quad (15)$$

<sup>3</sup>When selecting the direction cosines care must be taken that no two directions share the same absolute direction (e.g., invalid selection  $(1, 0, 0)$  and  $(-1, 0, 0)$ ).

<sup>4</sup>The Hilbert transform of the second derivative of the three-dimensional Gaussian function was approximated by finding the least squares fit to a third-order polynomial times a Gaussian [6].

<sup>5</sup>Matlab code for constructing the three-dimensional zone plate can be obtained from: <http://cvr.yorku.ca/members/gradstudents/kosta/Software>

Given the orientation and frequency selectivity of the filters, the zone plate was selected because it captures a continuum in both orientations and frequencies above and beyond those that the individual filters are selective for. In Fig. 2(a) a two-dimensional slice of the three-dimensional zone plate is presented. The rotated versions of the non-separable filters were arrived at by conducting the rotations in the continuous domain followed by discretization.

The sampling of the orientation of the filters were arrived at by representing the direction cosines  $(\alpha, \beta, \gamma)$  of the axis of symmetry parametrically by spherical coordinates  $(\theta, \phi, \rho = 1)$  as follows,

$$\begin{aligned}\alpha &= \cos(\theta)\sin(\phi) \\ \beta &= \sin(\theta)\sin(\phi) \\ \gamma &= \cos(\phi)\end{aligned}\tag{16}$$

For the experiment, both angles  $(\theta, \phi)$  were sampled at  $5^\circ$  intervals with the following bounds,  $0 \leq \theta \leq 2\pi$  and  $-\pi/2 \leq \phi \leq \pi/2$ , which corresponds to a sampling of a full sphere. Depicted in Fig. 2(b)-(g) are the convolutions of the  $G_2$  and  $H_2$  filters at various orientations with the three-dimensional zone plate.

The maximum rms errors for the  $G_2$  and  $H_2$  were found to be  $6.63 \times 10^{-13}$  and  $3.55 \times 10^{-12}$ , respectively. In Fig. 3(a) and Fig. 3(b) plots of the rms errors for the  $G_2$  and  $H_2$  filter are presented. The symmetrical nature of the rms error plots is due to the symmetrical nature of the filters in the frequency domain about the origin. The prominent minima of the  $H_2$  rms error correspond to the filters with a single non-zero coefficient  $k_i(\cdot)$ . The increased errors in the remaining filter outputs may be due to accumulation errors in the construction of the basis filters (i.e., more than one non-zero coefficient  $k_i(\cdot)$ ). Nonetheless the maximum error encountered is insignificant.

## 6 Example application

In this section a summary of a surveillance application is given that utilizes the steerable  $G_2$  and  $H_2$  filters detailed in Section 4.

A major problem with traditional approaches (e.g., difference imaging [4]) for surveillance of outdoor environments based on visual motion is that they are susceptible to distraction by irrelevant motions. Example distractions include, vegetation fluttering or swaying in the wind, specularities across water and clouds drifting across the sky.

With these difficulties in mind, in [20] (later extended in [21]) the author suggests a parsing of motion information that highlights salient regions relevant to the application of surveillance. The author observes that the time course that unimportant random and oscillatory motion events occur are small compared to the period that targets of interest maintain a coherent direction of movement. Given this observation the author suggests basing motion salience on the extent that a single coherent motion dominates local regions in the spatiotemporal domain. The author proposes using a set of directionally selective filters to capture the point-wise dominant direction in space-time. As an aside, there is evidence [7] that human vision finds salient structures jointly in space and time. In both [20, 21] measures of local direction are initially restricted to two-dimensional planes consisting of one spatial dimension ( $x$  or  $y$ ) and time  $t$ . These

measures are combined to make a final measure of motion salience. Rather, than analyze the spatiotemporal structure in separate slices in the discussion that follows we will analyze the three-dimensional structure directly. An advantage of analyzing the three-dimensional structure directly utilizing three-dimensional kernels (in our case the the  $G_2$  and  $H_2$  filters) is that they can provide a direct measure of motion not lying in either plane.

The first step consists of filtering the image sequence  $I(x, y, t)$  by the directionally selective filters  $G_2$  and  $H_2$  at orientations  $(\alpha, \beta, \gamma)_i$  (orientations specified below). Next, the filters are taken in quadrature to eliminate the phase sensitivity present in the output of each filter (see Appendix A). This produces a measure of local energy  $E_{(\alpha, \beta, \gamma)}(x, y, t)$ , within a frequency band,

$$E_{(\alpha, \beta, \gamma)}(x, y, t) = [G_{2(\alpha, \beta, \gamma)} * I(x, y, t)]^2 + [H_{2(\alpha, \beta, \gamma)} * I(x, y, t)]^2 \quad (17)$$

where  $*$  denotes the convolution operator. The resulting energy is a function of both orientation and contrast. To get a purer measure of orientation the response of each filter is normalized by the sum of the consort response, as follows,

$$\hat{E}_{(\alpha, \beta, \gamma)_i}(x, y, t) = \frac{E_{(\alpha, \beta, \gamma)_i}}{\sum_j E_{(\alpha, \beta, \gamma)_j}(x, y, t) + \epsilon} \quad (18)$$

where  $\epsilon$  is a small bias introduced to prevent instabilities when the overall pointwise energy estimate is negligible.

In [21] the author identifies six orientation patterns that have semantic interpretations; see Table 7 for a summary of the three-dimensional  $G_2/H_2$  filter orientation analogs of the two-dimensional filters presented in [21]. One case of interest are regions in the spatiotemporal domain that exhibit elongated structures (horizontal and vertical oriented spatial structures) parallel to the temporal axis when considered in X-T or Y-T spatiotemporal slices. In the frequency domain, these structures have their energy concentrated along the spatial frequency axis. This case is referred to as “static”. A second case identified is of a homogeneous spatial region where the intensity fluctuates over time. In the frequency domain the energy of this structure is concentrated on the temporal axis. This case is referred to as “flicker”. A third case is of a spatiotemporal region that exhibits coherent velocity in the X-T plane or Y-T plane. This region traces a slant in the spatiotemporal domain. In the frequency domain the energy also exhibits a slant about the origin. This case is referred to as “coherent motion” which includes rightward, leftward, upward and downward constant velocity motion. The use of the three-dimensional steerable filters allows us to elaborate this category by including constant velocity motion that does not lie strictly on the spatial coordinate axes.

The goal of this surveillance application is the extraction of coherently moving targets for subsequent tracking [5]. Figure 4 shows the energy outputs (upward, downward) of a synthetic image sequence consisting of a random dot square region moving 1 pixel/frame downward over a random dot background moving 1 pixel/frame upward. Figure 5 shows the energy outputs (rightward, static horizontal and static vertical) of a real world scene. Two people are walking away from each, one leftward the other rightward.

## 7 Summary

In this report the construction of three-dimensional separable steerable filters of the  $n$ th derivative of the Gaussian was presented. Additionally, as a proof of concept the second derivative of the Gaussian and its Hilbert transform, both in the continuous and discrete domains, were presented. Experimental evaluation shows that the error in the construction of the separable steerable second derivative of the Gaussian and Hilbert transform is negligible. Finally, an application of the  $G_2$  and  $H_2$  filters for surveillance was presented as an example of the filters' utility.

## References

- [1] E.H. Adelson and J.R. Bergen. Spatiotemporal energy models for the perception of motion. *Journal of the Optical Society of America-A*, 2(2):284–299, 1985.
- [2] R.N. Bracewell. *The Fourier Transform and Its Applications*. New York: McGraw-Hill, 2000.
- [3] P.E. Danielsson and O. Seger. Rotation invariance in gradient and higher order derivative detectors. *Computer Vision, Graphics and Image Processing*, 49(2):198–221, February 1990.
- [4] G.W. Donohoe, D.R. Hush, and N. Ahmed. Change detection for target detection and classification in video sequences. In *International Conference on Acoustics, Speech, and Signal Processing*, volume 21, pages 1084–1087, 1988.
- [5] M. Enzweiler, R. P. Wildes, and R. Herpers. Unified target detection and tracking using motion coherence. In *IEEE Motion*, 2005 (to appear).
- [6] W.T. Freeman and E.H. Adelson. The design and use of steerable filters. *IEEE Transactions on Pattern Analysis and Machine Intelligence*, 13(9):891–906, September 1991.
- [7] S. Gepshtein and M. Kubovy. The emergence of visual objects in space-time. In *National Academy of Sciences*, volume 97, pages 8186–8191, 2000.
- [8] H. Greenspan, S. Belongie, P. Perona, R. Goodman, S. Rakshit, and C. Anderson. Overcomplete steerable pyramid filters and rotation invariance. In *IEEE Conference on Computer Vision and Pattern Recognition*, pages 222–228, 1994.
- [9] R.M. Haralick. Digital step edges from zero crossing of second directional derivatives. *IEEE Transactions on Image Processing*, 11(1):58–68, January 1984.
- [10] C.L. Huang and Y.T. Chen. Motion estimation method using a 3D steerable filter. *Image and Vision Computing*, 13(1):21–32, February 1995.
- [11] M. Kass and A.P. Witkin. Analyzing oriented patterns. *Computer Vision, Graphics and Image Processing*, 37(3):362–385, March 1987.
- [12] H.E. Knutsson, R. Wilson, and G.H. Granlund. Anisotropic nonstationary image estimation and its applications part I: Restoration of noisy images. *IEEE Transactions on Communications*, 31:388–397, 1983.
- [13] J.J. Koenderink and A.J. van Doorn. Representation of local geometry in the visual system. *Biological Cybernetics*, 55(6):367–375, 1987.
- [14] R. Lenz. *Group Theoretic Methods in Image Processing*. New York: Springer-Verlag, 1990.
- [15] P. Perona. Deformable kernels for early vision. *IEEE Transactions on Pattern Analysis and Machine Intelligence*, 17(5):488–499, May 1995.

- [16] K.H. Rosen. *Discrete Mathematics and its Applications*. Boston: McGraw-Hill, 1998.
- [17] D. Shy and P. Perona. X-Y separable pyramid steerable scalable kernels. In *IEEE Conference on Computer Vision and Pattern Recognition*, pages 237–244, 1994.
- [18] E.P. Simoncelli and W.T. Freeman. The steerable pyramid: A flexible architecture for multi-scale derivative computation. In *International Conference on Image Processing*, pages 444–447, 1995.
- [19] E.W. Weisstein. *CRC Concise Encyclopedia of Mathematics*. Boca Raton: Chapman and Hall/CRC, 2003.
- [20] R.P. Wildes. A measure of motion salience for surveillance applications. In *IEEE International Conference on Image Processing*, pages 183–187, 1988.
- [21] R.P. Wildes and Bergen J.R. Qualitative spatiotemporal analysis using an oriented energy representation. In *European Conference on Computer Vision*, 2000.
- [22] W. Yu, K. Daniilidis, and G. Sommer. Approximate orientation steerability based on angular gaussians. *IEEE Transactions on Image Processing*, 10(2):193–205, February 2001.

## A Local energy

In this section the local energy extracted from a cosinusoidal signal using the quadrature outputs of the  $G_2$  (i.e.,  $\frac{\partial^2}{\partial t^2}G(t)$ ) and  $H_2$  (i.e., the Hilbert transform of  $G_2$ ) filters will be derived. Note that local energy as derived below is exact only for a pure sinusoidal signal.

The output of the  $G_2$  filtering process is formalized as follows,

$$\frac{\partial^2}{\partial t^2}G(t) * A\cos(\omega t) = AG(t) * \frac{\partial^2}{\partial t^2}\cos(\omega t) \quad (19)$$

$$= -G(t) * A\omega^2\cos(\omega t) \quad (20)$$

$$= -mA\omega^2\cos(\omega t) \quad (21)$$

where  $*$  represents the convolution operator,  $A$  and  $\omega$  denote the amplitude and frequency of the input signal, respectively, and  $m$  is a constant from the modulation transfer function (MTF) of  $G(t)$ .

The Hilbert transform  $H[\cdot]$  introduces a phase shift of  $\pi/2$  to every frequency of a signal [2]. The Hilbert transform of Eq. (19) yields,

$$H\left[\frac{\partial^2}{\partial t^2}G(t) * A\cos(\omega t)\right] = H\left[AG(t) * \frac{\partial^2}{\partial t^2}\cos(\omega t)\right] \quad (22)$$

$$= H\left[-mA\omega^2\cos(\omega t)\right] \quad (23)$$

$$= -mA\omega^2\cos(\omega t + \pi/2) \quad (24)$$

$$= -mA\omega^2\sin(\omega t) \quad (25)$$

Taking the  $G_2$  (Eq. (21)) and  $H_2$  (Eq. (25)) filter outputs in quadrature, yields,

$$[-mA\omega^2\cos(\omega t)]^2 + [-mA\omega^2\sin(\omega t)]^2 = m^2A^2\omega^4[\cos(\omega t)^2 + \sin(\omega t)^2] \quad (26)$$

$$= m^2A^2\omega^4[1] \quad (27)$$

$$= m^2A^2\omega^4 \quad (28)$$

Therefore, the local energy is a function of the amplitude  $A$ , frequency  $\omega$  of the input signal and the distance of the input signal's frequency with respect to the optimal tuning of the  $G_2$  and  $H_2$  filters.

Basis		Interpolation	
$G_{2a}$	$= N(2x^2 - 1)e^{-(x^2+y^2+z^2)}$	$k(\alpha, \beta, \gamma)$	$= \alpha^2$
$G_{2b}$	$= N(2xy)e^{-(x^2+y^2+z^2)}$	$k(\alpha, \beta, \gamma)$	$= 2\alpha\beta$
$G_{2c}$	$= N(2y^2 - 1)e^{-(x^2+y^2+z^2)}$	$k(\alpha, \beta, \gamma)$	$= \beta^2$
$G_{2d}$	$= N(2xz)e^{-(x^2+y^2+z^2)}$	$k(\alpha, \beta, \gamma)$	$= 2\alpha\gamma$
$G_{2e}$	$= N(2yz)e^{-(x^2+y^2+z^2)}$	$k(\alpha, \beta, \gamma)$	$= 2\beta\gamma$
$G_{2f}$	$= N(2z^2 - 1)e^{-(x^2+y^2+z^2)}$	$k(\alpha, \beta, \gamma)$	$= \gamma^2$

Table 1: X-Y-Z separable basis set and interpolation functions for the second derivative of the Gaussian.  $N$  is a normalization constant equaling  $\frac{2}{\sqrt{3}}(\frac{2}{\pi})^{3/4}$ , introduced so that the integral over all space of the square of the function equals one. To construct a second derivative of a Gaussian where the axis of symmetry (i.e., X-axis) is mapped to the direction cosine  $\Omega = (\alpha, \beta, \gamma)$ , use  $G_2^\Omega = \sum_{i \in \{a, \dots, f\}} k_i(\Omega) G_{2i}$ .

	1D Function	Tap #				
		0	1	2	3	4
f1	$N(2t^2 - 1)e^{-t^2}$	-0.8230	-0.0537	0.3540	0.1025	0.0084
f2	$e^{-t^2}$	1.0000	0.6383	0.1660	0.0176	0.0008
f3	$2Nte^{-t^2}$	0	0.7039	0.3662	0.0582	0.0034
f4	$te^{-t^2}$	0	0.4277	0.2225	0.0354	0.0020

Table 2: 9-tap filters for X-Y-Z separable basis set for  $G_2$ . Filters f1 and f2 have even symmetry; f3 and f4 have odd symmetry. These filters were taken from Table 1, with a sample spacing of 0.67.

$G_2$ Basis Filter	Filter in X	Filter in Y	Filter in Z
$G_{2a}$	f1	f2	f2
$G_{2b}$	f3	f4	f2
$G_{2c}$	f2	f1	f2
$G_{2d}$	f3	f2	f4
$G_{2e}$	f2	f3	f4
$G_{2f}$	f2	f2	f1

Table 3:  $G_2$  basis filters. Summarized is the construction of the  $G_2$  basis filters (a-f) using the filters given in Table 2.

Basis		Interpolation	
$H_{2a}$	$= N(x^3 - 2.254x)e^{-(x^2+y^2+z^2)}$	$k(\alpha, \beta, \gamma)$	$= \alpha^3$
$H_{2b}$	$= Ny(x^2 - 0.751333)e^{-(x^2+y^2+z^2)}$	$k(\alpha, \beta, \gamma)$	$= 3\alpha^2\beta$
$H_{2c}$	$= Nx(y^2 - 0.751333)e^{-(x^2+y^2+z^2)}$	$k(\alpha, \beta, \gamma)$	$= 3\alpha\beta^2$
$H_{2d}$	$= N(y^3 - 2.254y)e^{-(x^2+y^2+z^2)}$	$k(\alpha, \beta, \gamma)$	$= \beta^3$
$H_{2e}$	$= Nz(x^2 - 0.751333)e^{-(x^2+y^2+z^2)}$	$k(\alpha, \beta, \gamma)$	$= 3\alpha^2\gamma$
$H_{2f}$	$= Nxyz e^{-(x^2+y^2+z^2)}$	$k(\alpha, \beta, \gamma)$	$= 6\alpha\beta\gamma$
$H_{2g}$	$= Nz(y^2 - 0.751333)e^{-(x^2+y^2+z^2)}$	$k(\alpha, \beta, \gamma)$	$= 3\beta^2\gamma$
$H_{2h}$	$= Nx(z^2 - 0.751333)e^{-(x^2+y^2+z^2)}$	$k(\alpha, \beta, \gamma)$	$= 3\alpha\gamma^2$
$H_{2i}$	$= Ny(z^2 - 0.751333)e^{-(x^2+y^2+z^2)}$	$k(\alpha, \beta, \gamma)$	$= 3\beta\gamma^2$
$H_{2j}$	$= N(z^3 - 2.254z)e^{-(x^2+y^2+z^2)}$	$k(\alpha, \beta, \gamma)$	$= \gamma^3$

Table 4: X-Y-Z separable basis set and interpolation functions for fit to Hilbert transform of the second derivative of the Gaussian.  $N$  is a normalization constant equaling 0.877776, introduced so that the integral over all space of the square of the function equals one. To construct a second derivative of a Gaussian where the axis of symmetry (i.e., X-axis) is mapped to the direction cosine  $\Omega = (\alpha, \beta, \gamma)$ , use  $H_2^\Omega = \sum_{i \in \{a, \dots, j\}} k_i(\Omega) H_{2i}$ .

	1D Function	Tap #				
		0	1	2	3	4
f1	$N(t^3 - 2.254t)e^{-t^2}$	0	-0.6776	-0.0895	0.0554	0.0088
f2	$N(t^2 - 0.751333)e^{-t^2}$	-0.6595	-0.1695	0.1522	0.0508	0.0043
f3	$e^{-t^2}$	1.0000	0.6383	0.1660	0.0176	0.0008
f4	$Nte^{-t^2}$	0	0.3754	0.1953	0.0310	0.0018
f5	$te^{-t^2}$	0	0.4277	0.2225	0.0354	0.0020

Table 5: 9-tap filters for X-Y-Z separable basis set for  $H_2$ . Filters f2 and f3 have even symmetry; f1, f4 and f5 have odd symmetry. These filters were taken from Table 4, with a sample spacing of 0.67.

$H_2$ Basis Filter	Filter in X	Filter in Y	Filter in Z
$H_{2a}$	f1	f3	f3
$H_{2b}$	f2	f5	f3
$H_{2c}$	f5	f2	f3
$H_{2d}$	f3	f1	f3
$H_{2e}$	f2	f3	f5
$H_{2f}$	f4	f5	f5
$H_{2g}$	f3	f2	f5
$H_{2h}$	f5	f3	f2
$H_{2i}$	f3	f5	f2
$H_{2j}$	f3	f3	f1

Table 6:  $H_2$  basis filters. Summarized is the construction of the  $H_2$  basis filters (a-j) using the filters given in Table 5.

Category	orientation $(\alpha, \beta, \gamma)$
static vertical	$(1, 0, 0)$
static horizontal	$(0, 1, 0)$
flicker	$(0, 0, 1)$
rightward	$(1/\sqrt{2}, 0, 1/\sqrt{2})$
leftward	$(-1/\sqrt{2}, 0, 1/\sqrt{2})$
upward	$(0, 1/\sqrt{2}, 1/\sqrt{2})$
downward	$(0, -1/\sqrt{2}, 1/\sqrt{2})$

Table 7: Summarized are the orientations (i.e., direction cosines) of the  $G_2/H_2$  filters for isolating the energy of the corresponding motion categories.

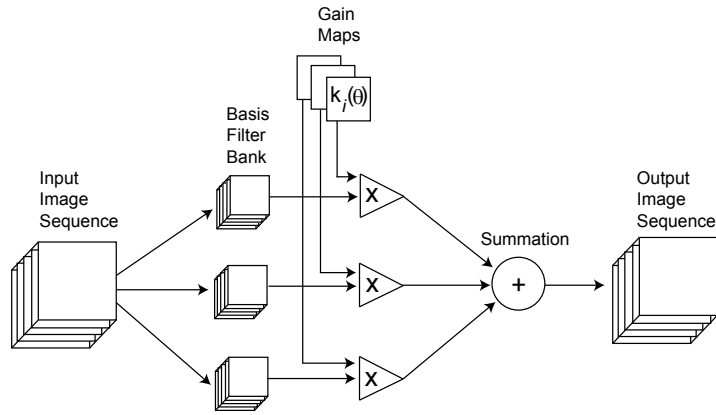
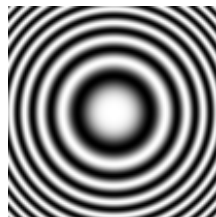


Figure 1: Three-dimensional steerable filter architecture. Adapted from [6].



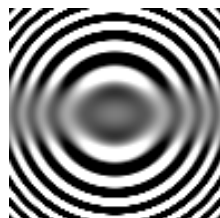
(a) zone plate



(b)  $G_2$ : (1, 0, 0)



(c)  $H_2$ : (1, 0, 0)



(d)  $G_2$ : (0, 1, 0)



(e)  $H_2$ : (0, 1, 0)

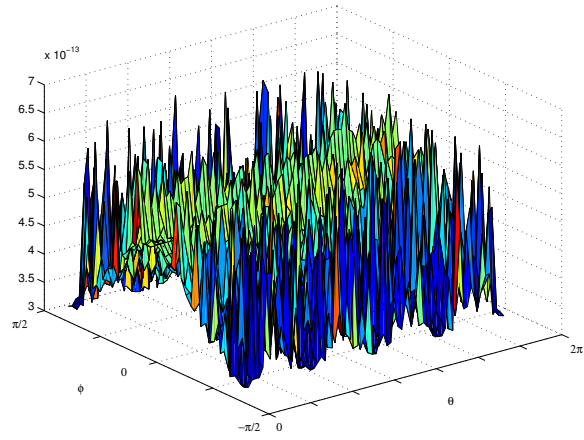


(f)  $G_2$ : (1, 1, 0)

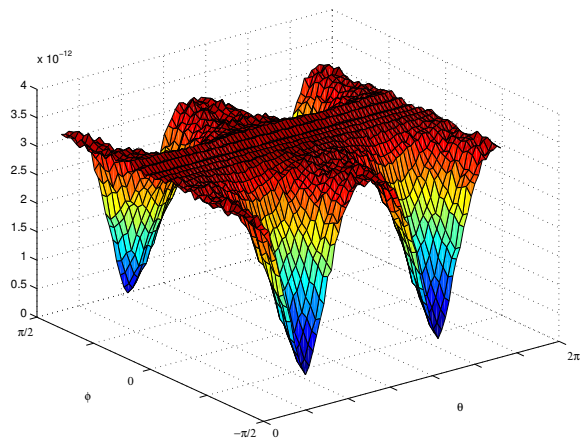


(g)  $H_2$ : (1, 1, 0)

Figure 2: Filtered zone plate. Depicted is (a) an X-Y slice from a three-dimensional zone plate and (b)-(g) various corresponding  $G_2/H_2$  filtered X-Y slices. The accompanying triples in the captions of the filtered outputs represent the direction of the axis of symmetry.

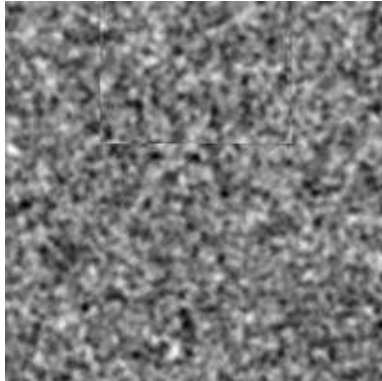


(a)  $G_2$  rms error

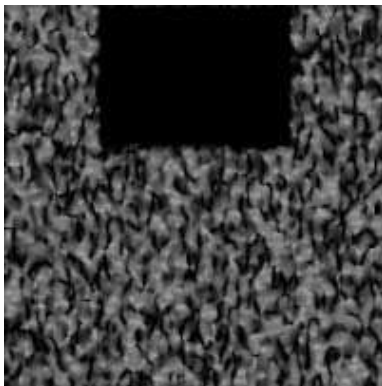


(b)  $H_2$  rms error

Figure 3:  $G_2/H_2$  rms errors.



(a) Intensity image



(b) Upward energy



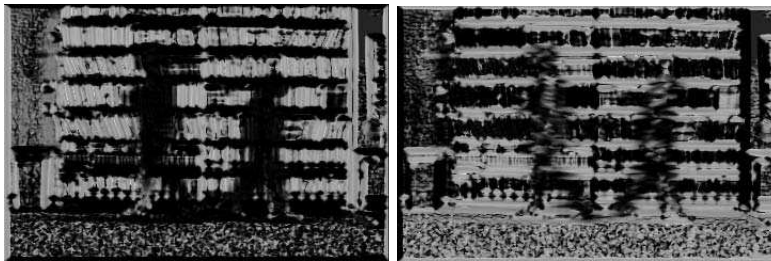
(c) Downward energy

Figure 4: Energy images from a synthetic image sequence. (a) a frame taken from synthetic image sequence of a random dot foreground square region moving downwards 1 pixel/frame over a random dot background moving upward 1 pixel/frame (b) the upward normalized energy and (c) the downward normalized energy.



(a) Intensity image

(b) Rightward energy



(c) Static vertical energy

(d) Static horizontal energy

Figure 5: Energy images from an indoor scene. (a) a frame taken from scene of two people walking away from each other, one rightward and the other leftward (b) the rightward normalized energy (c) the energy attributed to static structures oriented spatially vertically and (d) the energy attributed to static structures oriented spatially horizontally.